

Continuous-Time Quantum Monte Carlo Study of Local Non-Fermi Liquid State in the Multichannel Anderson Model

Junya Otsuki*

Department of Physics, Tohoku University, Sendai 980-8578

The impurity Green's function G_f in the local non-Fermi liquid state is evaluated by means of the continuous-time quantum Monte Carlo method extended to the multichannel Anderson model. For $N = M$ (where N and M are numbers of spin components and channels, respectively), G_f is expressed as $-\text{Im}G_f(\omega + i0) = c - b|\omega|^{1/2}$, and the zero-frequency value c depends only on $N (= M)$. A corresponding impurity self-energy at low frequencies is composed of two parts: a resonance term related to c , and a non-Fermi liquid term proportional to $|\omega|^{1/2}$. The characteristic energy scale is discussed in terms of the non-Fermi liquid term in the self-energy.

KEYWORDS: continuous-time quantum Monte Carlo (CT-QMC), two-channel Kondo effect

1. Introduction

The multichannel Kondo effect is a typical example that leads to a local non-Fermi liquid ground state.¹⁾ It has been recognized that the peculiar low-temperature behaviors observed in uranium compounds and metals with uranium impurities are due to the two-channel Kondo effect.²⁾ This kind of non-Fermi liquid state has been investigated from a more general point of view based on models generalized to $SU(N) \otimes SU(M)$ symmetry.³⁾ Then, their critical nature has been discussed extensively.^{4,5)}

Regarding the (single-channel) Kondo problem, the Anderson Hamiltonian gives clear insight:^{6,7)} the ground state is connected to that in the non-interacting limit. In this analogy, the multichannel Kondo effect can be addressed based on an Anderson Hamiltonian.⁸⁾ The inclusion of the impurity charge degree of freedom enables us to describe the local dynamics via the impurity Green's function. We thus consider the $SU(N) \otimes SU(M)$ multichannel Anderson model given by²⁾

$$\mathcal{H} = \sum_{\mathbf{k}\alpha\mu} \epsilon_{\mathbf{k}} c_{\mathbf{k}\alpha\mu}^\dagger c_{\mathbf{k}\alpha\mu} + E_{\text{ex}} \sum_{\alpha} X_{\alpha,\alpha} + V \sum_{\alpha\mu} (X_{\mu,-\alpha} c_{\alpha\mu} + \text{h.c.}). \quad (1)$$

The (pseudo-)spin index μ and channel index α run over N and M components, respectively. The f^2 state $|\mu\rangle$ forms a channel singlet ($-\alpha$ denotes the counterpart of α), and the f^1 state $|\alpha\rangle$ has the energy E_{ex} relative to $|\mu\rangle$. The Hilbert space of f states is restricted to $|\alpha\rangle$ and $|\mu\rangle$ by using the X -operators $X_{\gamma,\gamma'} = |\gamma\rangle\langle\gamma'|$ with $\gamma = \alpha, \mu$, on which $\sum_{\gamma} X_{\gamma,\gamma} = 1$ is imposed. $c_{\alpha\mu} = N_0^{-1/2} \sum_{\mathbf{k}} c_{\mathbf{k}\alpha\mu}$ with N_0 being number of sites. The M -channel Coqblin-Schrieffer model is derived from the Hamiltonian (1) as a localized limit V^2 , $E_{\text{ex}} \rightarrow \infty$ with V^2/E_{ex} fixed. Exact thermodynamics of the model (1)⁹⁾ as well as the localized limit⁵⁾ has been derived.

Concerning the dynamical properties, a two-channel case, $N = M = 2$, has been clarified by the numerical renormalization group¹⁰⁾ and by an exact method.¹¹⁾ Gen-

eral cases have been investigated by perturbational treatments.^{3,12,13)} In this paper, we numerically investigate the dynamical properties of the multichannel Anderson model. To this end, we develop an algorithm based on the recently developed continuous-time quantum Monte Carlo (CT-QMC) method,¹⁴⁻¹⁶⁾ which is explained in the next section. We show numerical results for the impurity Green's function and self-energy in §3.

2. CT-QMC for the multichannel Anderson model

We study the model (1) by the CT-QMC, which evaluates a perturbation expansion stochastically. In the present case, we adopt the hybridization expansion.¹⁵⁾ Since the non-perturbative part is diagonal with respect to α and μ , the efficient algorithm using a 'segment' picture is applicable by a slight modification. Figure 1 shows a diagram of a configuration of order V^6 . Spin states μ_i and channel states α_i appear alternately, which are hereafter referred to as segment and anti-segment, respectively. In general, a configuration of order V^{2k} is represented by $q_k \equiv \{\tau_i, \tau'_i, \alpha_i, \mu_i\}$. The trace over the local states is thus taken into account graphically. On the other hand, the trace over conduction electrons is evaluated based on Wick's theorem. A Monte Carlo sampling is performed in the configuration space composed of k and q_k .

We perform the following update processes: (i) addition/removal of a segment or an anti-segment, and (ii) exchange of spin or channel indices. Fig. 2(a) shows the addition of a segment. The index μ of the segment is randomly chosen, and accordingly the update probability differs from that in ref. 15 by a factor of N . When either N or M is larger than 2, the ergodicity is not satisfied only by process (i). For

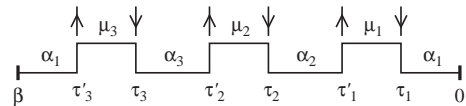


Fig. 1. Diagrammatic representation of a configuration of order V^6 . The outgoing and incoming arrows indicate creation and annihilation of conduction electrons, respectively.

*E-mail address: otsuki@cmpt.phys.tohoku.ac.jp

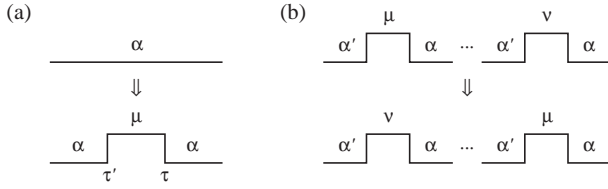


Fig. 2. Update processes: (a) addition of a segment, and (b) exchange of spin indices.

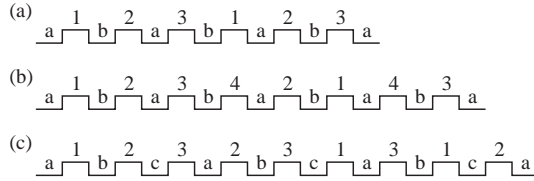


Fig. 3. Examples of diagrams which cannot be reached without the ‘exchange’ process. The spin and channel components are labeled as 1, 2, ..., and a, b, ..., respectively.

example, configurations shown in Fig. 3 cannot be reached. This problem can be solved by introducing a process shown in Fig. 2(b), which exchanges the spin indices. We perform a similar update to exchange the channel indices as well.

In the simulation, we observe negative weight configurations for $N = M > 2$. However, since their contribution is less than 10% in the parameter range shown in this paper, the sign problem has little effect on the simulation.

3. Numerical Results

In this paper, we restrict ourselves to $N = M$. We use a rectangular density of states $\rho(\epsilon) = (1/2D)\theta(D - |\epsilon|)$ for conduction electrons with $D = 1$. We fix $NV^2 = 0.12$ so that the exponent of the Kondo temperature is the same for different N . The width of the localized state $\Delta = \pi V^2 \rho(0)$ is $\Delta \simeq 0.094$ at most (for $N = 2$), and therefore the effect of finite band width may be neglected.

3.1 Green’s function

We first show results for the single-particle Green’s function G_f , which is defined in the restricted Hilbert space by

$$G_f(i\epsilon_n) = - \int_0^\beta d\tau \langle X_{-\alpha, \mu}(\tau) X_{\mu, -\alpha} \rangle e^{i\epsilon_n \tau}, \quad (2)$$

where $\epsilon_n = (2n + 1)\pi T$ is the fermionic Matsubara frequency. At high frequencies, G_f follows $G_f(i\epsilon_n) \sim a/i\epsilon_n$ with $a < 1$, since the Hilbert space is restricted. The a varies between $1/N$ and $1/M$ depending on E_{ex} , and in a special case of $N = M$, $a = 1/N$.

In Fig. 4, $-\text{Im}G_f(i\epsilon_n)\Delta$ is plotted against $\sqrt{\epsilon_n}$ for $E_{\text{ex}} = 0$. For all $N = M$, G_f is expressed as $-\text{Im}G_f(i\epsilon_n) = c - b\sqrt{\epsilon_n}$ at low frequencies. Hence, $G_f(z)$ is non-analytic at $z \rightarrow +i0$, and the spectrum $-\text{Im}G_f(\omega + i0)$ on real frequencies exhibits a cusp structure expressed by $c - b|\omega|^{1/2}$, which has been reported for $N = M = 2$.^{4,10,11} The value c at $\epsilon_n \rightarrow +0$ decreases with increasing N . From Fig. 4 and an analogy with the Friedel sum-rule in the Fermi liquid, we

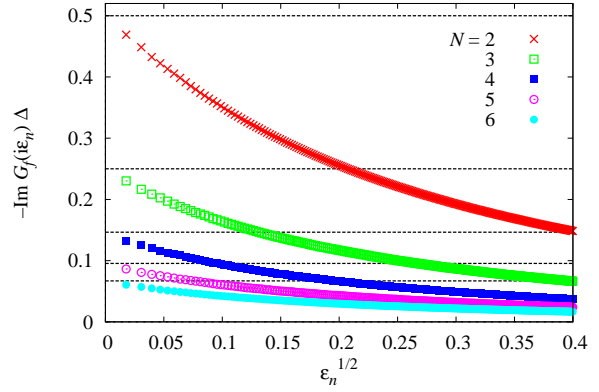


Fig. 4. (Color online) The imaginary part of the Green’s function $G_f(i\epsilon_n)$ for $N = M$, $NV^2 = 0.12$, $E_{\text{ex}} = 0$ and $T = 0.0001$. The lines show $\sin^2(\pi/2N)$.

conjecture the following relation:

$$-\text{Im}G_f(+i0) = \frac{1}{\Delta} \sin^2\left(\frac{\pi}{2N}\right), \quad (3)$$

which is indicated in Fig. 4. Eq. (3) includes the result for $N = M = 2$,^{4,10,11} $1/(2\Delta)$, and reduces to the result in the non-crossing approximation,³ $\pi^2/[(N + M)^2\Delta]$, in the limit $N = M \gg 2$. For $E_{\text{ex}} = 0$, the particle-hole symmetry leads to $\text{Re}G_f(i\epsilon_n) = 0$, meaning that the phase shift ϕ of conduction electrons at $\omega = 0$ is fixed at $\phi = \pi/2$ irrespective of the value of $N = M$. Hence, the sine factor in eq. (3) is not connected with ϕ but is due to the imaginary part of the self-energy.

3.2 Self-Energy

We discuss the self-energy in the restricted Hilbert space. The self-energy $\Sigma_f(i\epsilon_n)$ in the ordinary definition is given by

$$G_f(i\epsilon_n) = \frac{1}{i\epsilon_n - \epsilon_f - \Gamma(i\epsilon_n) - \Sigma_f(i\epsilon_n)}, \quad (4)$$

where $\Gamma(i\epsilon_n) = N_0^{-1} \sum_{\mathbf{k}} V^2 / (i\epsilon_n - \epsilon_{\mathbf{k}})$. In the restricted Hilbert space, $\Sigma_f(i\epsilon_n)$ diverges according to $\Sigma_f(i\epsilon_n) \sim i\epsilon_n(1 - 1/a)$ at $\epsilon_n \rightarrow \infty$, since $G_f(i\epsilon_n) \sim a/i\epsilon_n$ with $a < 1$. Although this divergence does not produce any problem with analysis of low-energy properties, it is not convenient in practice. Thus, we define an alternative self-energy $\tilde{\Sigma}_f$ as follows:

$$G_f(i\epsilon_n) = \frac{a}{i\epsilon_n - \tilde{\epsilon}_f - a\Gamma(i\epsilon_n) - \tilde{\Sigma}_f(i\epsilon_n)}. \quad (5)$$

$\tilde{\Sigma}_f$ is related to the ordinary self-energy Σ_f by $\tilde{\Sigma}_f = a\Sigma_f + i\epsilon_n(1 - a) - (\tilde{\epsilon}_f - a\epsilon_f)$, and converges in proportion to $1/i\epsilon_n$ at high frequencies. By using $\tilde{\Sigma}_f$, for example, the renormalization factor z in the Fermi-liquid state is evaluated as

$$z = [1 - \partial \text{Im}\Sigma_f(i\epsilon_n) / \partial \epsilon_n]_{\epsilon_n \rightarrow +0}^{-1} = a[1 - \partial \text{Im}\tilde{\Sigma}_f(i\epsilon_n) / \partial \epsilon_n]_{\epsilon_n \rightarrow +0}^{-1} \equiv a\tilde{z}. \quad (6)$$

\tilde{z} stands for a quasi-particle weight within the restricted Hilbert space, and accordingly $\tilde{\Sigma}_f$ in eq. (5) may be a reasonable definition.

Figure 5(a) shows $-\text{Im}\tilde{\Sigma}_f(i\epsilon_n)$ divided by $a\Delta$ as a func-

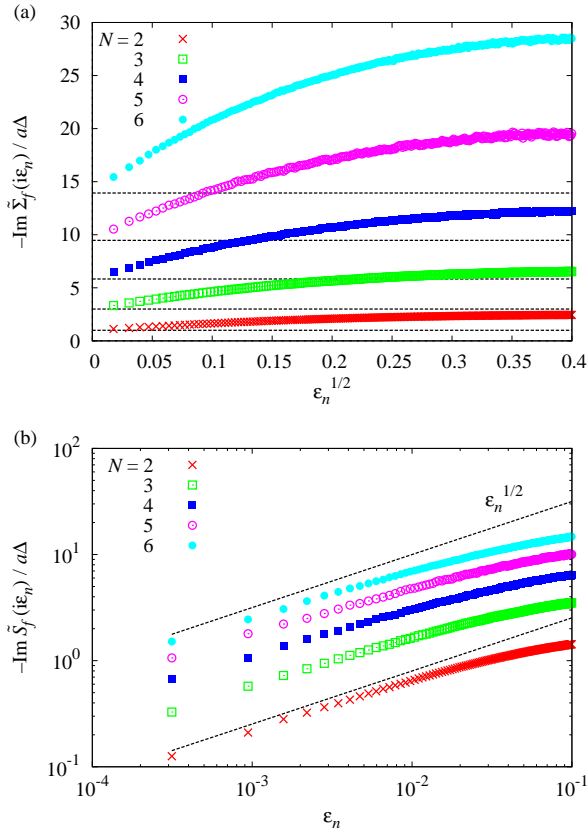


Fig. 5. (Color online) (a) The imaginary part of the self-energy $\tilde{\Sigma}_f(i\epsilon_n)$ defined by eq. (5). The lines show $\cot^2(\pi/2N)$. (b) $\tilde{S}_f(i\epsilon_n) = \tilde{\Sigma}_f(i\epsilon_n) - \xi a \Gamma(i\epsilon_n)$ on a log-log scale. The parameters are the same as in Fig. 4.

tion of $\sqrt{\epsilon_n}$. Similarly to $G_f(i\epsilon_n)$, $\tilde{\Sigma}_f(i\epsilon_n)$ includes a term proportional to $\sqrt{\epsilon_n}$ in the limit $\epsilon_n \rightarrow +0$, and converges to a finite value. To separate the zero-frequency value from $\tilde{\Sigma}_f$, we introduce a parameter ξ as follows:

$$\tilde{\Sigma}_f(i\epsilon_n) = \xi a \Gamma(i\epsilon_n) + \tilde{S}_f(i\epsilon_n). \quad (7)$$

ξ is determined so that $\text{Im}\tilde{S}_f(+i0) = 0$. For $N = M$, noting that $\text{Re}G_f(i\epsilon_n) = 0$, we obtain from eq. (3)

$$\xi = \cot^2\left(\frac{\pi}{2N}\right). \quad (8)$$

In the case of $N = M = 2$, $\tilde{S}_f(i\epsilon_n)$ eventually corresponds to the self-energy discussed in refs. 10 and 11. Figure 5(b) shows $\tilde{S}_f(i\epsilon_n)$ on a log-log scale. We can clearly see the power-law behavior $-\text{Im}\tilde{S}_f(i\epsilon_n) \propto |\epsilon_n|^{1/2}$, which means $-\text{Im}\tilde{S}_f(\omega + i0) \propto |\omega|^{1/2}$.

3.3 Effect of Level Splitting E_{ex} : Energy Scale

So far, we have examined $E_{\text{ex}} = 0$. We now discuss the effect of E_{ex} . In refs. 10 and 11, it is reported for $N = M = 2$ that $\text{Im}G_f(+i0)$ and $\text{Im}\tilde{\Sigma}_f(+i0)$ do not depend on E_{ex} . We have confirmed for $N = M \geq 2$ that eqs. (3) and (8) hold up to $E_{\text{ex}} = 0.3$ within numerical accuracy. The finite value of E_{ex} causes an asymmetry of the cusp keeping the value at $\omega = 0$: $c + b|\omega|^{1/2}$ changes into $c + [b_+\theta(\omega) + b_-\theta(-\omega)]|\omega|^{1/2}$.

As E_{ex} increases, the energy scale becomes smaller. We

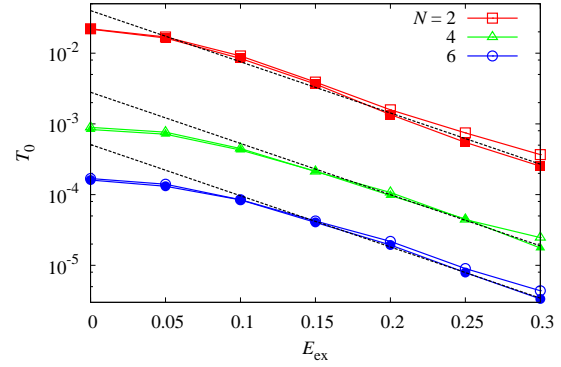


Fig. 6. (Color online) A characteristic energy scale T_0 defined in eq. (9) as a function of E_{ex} . T_0 is evaluated from $\tilde{S}_f(i\epsilon_0)$ at $T = 0.0005$ (open symbols) and $T = 0.00025$ (closed symbols). The lines show $\exp[-E_{\text{ex}}/NV^2\rho(0)]$.

define a characteristic energy scale T_0 in terms of \tilde{S}_f by

$$-\text{Im}\tilde{S}_f(i\epsilon_n)/a\Delta \sim (\epsilon_n/T_0)^{1/2}, \quad (9)$$

in the limit $\epsilon_n \rightarrow 0$. Because T_0 may be defined with an arbitrary factor, we shall discuss only its exponent. In Fig. 6, we show T_0 as a function of E_{ex} . T_0 follows $T_0 \propto T_K \propto \exp(-1/g)$ with $g = NV^2\rho(0)/E_{\text{ex}}$ for $E_{\text{ex}} \gtrsim 0.15$, namely $g \lesssim 0.4$. We conclude that the exponent of the energy scale of the non-Fermi liquid self-energy agrees with the Kondo temperature T_K in the corresponding single-channel model.

4. Summary

We have presented the impurity Green's function $G_f(i\epsilon_n)$ and the self-energy $\tilde{\Sigma}_f(i\epsilon_n)$ in the non-Fermi liquid state using the CT-QMC extended to the multichannel Anderson model. For $N = M$, G_f and $\tilde{\Sigma}_f$ are non-analytic at $\omega = 0$ as $|\omega|^{1/2}$. The zero-frequency spectrum $\text{Im}G_f(+i0)$ does not depend on the excitation energy E_{ex} , and correspondingly $\text{Im}\tilde{\Sigma}_f(+i0)$ has a finite value. These values depend only on $N (= M)$, and seem to be expressed as eqs. (3), (7) and (8). An analysis of general N, M is left for future work.

We acknowledge Prof. Y. Kuramoto for comments on the manuscript. This work was supported by a Grant-in-Aid for Scientific Research on Innovative Areas ‘‘Heavy Electrons’’ (No. 20102008) of the Ministry of Education, Culture, Sports, Science, and Technology, Japan.

- 1) P. Nozières and A. Blandin: J. Phys. (Paris) **41** (1980) 193.
- 2) D. L. Cox and A. Zawadowski: Adv. Phys. **47** (1998) 599.
- 3) D. L. Cox and A. E. Ruckenstein: Phys. Rev. Lett. **71** (1993) 1613.
- 4) A. W. W. Ludwig and I. Affleck: Phys. Rev. Lett. **67** (1991) 3160; I. Affleck and A. W. W. Ludwig: Phys. Rev. B **48** (1993) 7297.
- 5) A. Jerez, N. Andrei, and G. Zaránd: Phys. Rev. B **58** (1998) 3814.
- 6) K. Yamada: *Electron Correlation in Metals* (Cambridge University Press, Cambridge, U.K., 2004).
- 7) K. Yosida: *Theory of Magnetism* (Springer-Verlag, Berlin, 1996).
- 8) A. Schiller, F. B. Anders, and D. L. Cox: Phys. Rev. Lett. **81** (1998) 3235.
- 9) C. J. Bolech and N. Andrei: Phys. Rev. B **71** (2005) 205104.
- 10) F. B. Anders: Phys. Rev. B **71** (2005) 121101.
- 11) H. Johannesson, C. J. Bolech and N. Andrei: Phys. Rev. B **71** (2005) 195107.
- 12) J. Kroha, P. Wölfle, and T. A. Costi: Phys. Rev. Lett. **79** (1997) 261; J.

- Kroha and P. Wölfle: Acta Phys. Pol. B **29** (1998) 3781.
- 13) A. Tsuruta, Y. Ōno, T. Matsuura, and Y. Kuroda: J. Phys. Soc. Jpn. **66** (1997) 3528.
- 14) A.N. Rubtsov, V.V. Savkin and A.I. Lichtenstein: Phys. Rev. B **72** (2005) 035122.
- 15) P. Werner, A. Comanac, L.de' Medici, M. Troyer and A.J. Millis: Phys. Rev. Lett. **97** (2006) 076405; P. Werner and A.J. Millis: Phys. Rev. B **74** (2006) 155107.
- 16) J. Otsuki, H. Kusunose, P. Werner and Y. Kuramoto: J. Phys. Soc. Jpn. **76** (2007) 114707.